

Effects of B segregation on Mo-rich phase precipitation in S31254 super-austenitic stainless steels: Experimental and first-principles study

Pan-Pan Xu(徐攀攀), Jin-Yao Ma(马晋遥), Zhou-Hua Jiang(姜周华), Yi Zhang(张翊), Chao-Xiong Liang(梁超雄), Nan Dong(董楠), and Pei-De Han(韩培德)

Citation: Chin. Phys. B, 2022, 31 (**11**): 116402. DOI: 10.1088/1674-1056/ac744a

What follows is a list of articles you may be interested in

Effect of Mo doping on phase change performance of Sb_2Te_3

Wan-Liang Liu(刘万良), Ying Chen(陈莹), Tao Li(李涛), Zhi-Tang Song(宋志棠), and Liang-Cai Wu(吴良才)

Chin. Phys. B, 2021, 30 (**8**): 086801. DOI: 10.1088/1674-1056/abe22d

Effects of WC-Co reinforced Ni-based alloy by laser melting deposition: Wear resistance and corrosion resistance

Zhao-Zhen Huang(黄昭祯), Zhi-Chen Zhang(张志臣), Fan-Liang Tantai(澹台凡亮), Hong-Fang Tian(田洪芳), Zhen-Jie Gu(顾振杰), Tao Xi(郗涛), Zhu Qian(钱铸), and Yan Fang(方艳)

Chin. Phys. B, 2021, 30 (**1**): 016802. DOI: 10.1088/1674-1056/abb223

Effect of scanning speeds on electrochemical corrosion resistance of laser cladding TC4 alloy

Xiaotian Feng(冯晓甜), Jianbo Lei(雷剑波), Hong Gu(顾宏), Shengfeng Zhou(周圣丰)

Chin. Phys. B, 2019, 28 (**2**): 026802. DOI: 10.1088/1674-1056/28/2/026802

Metastable phase separation and rapid solidification of undercooled $Co_{40}Fe_{40}Cu_{20}$ alloy

Xiaojun Bai(白晓军), Yaocen Wang(汪姚岑), Chongde Cao(曹崇德)

Chin. Phys. B, 2018, 27 (**11**): 116402. DOI: 10.1088/1674-1056/27/11/116402

Direct characterization of boron segregation at random and twin grain boundaries

Xiang-Long Li(李向龙), Ping Wu(吴平), Rui-Jie Yang(杨锐杰), Shi-Ping Zhang(张师平), Sen Chen(陈森), Xue-Min Wang(王学敏), Xiu-Lan Huai(淮秀兰)

Chin. Phys. B, 2017, 26 (**8**): 086802. DOI: 10.1088/1674-1056/26/8/086802

Effects of B segregation on Mo-rich phase precipitation in S31254 super-austenitic stainless steels: Experimental and first-principles study

Pan-Pan Xu(徐攀攀)[1], Jin-Yao Ma(马晋遥)[1,2,†], Zhou-Hua Jiang(姜周华)[4], Yi Zhang(张翊)[1], Chao-Xiong Liang(梁超雄)[1], Nan Dong(董楠)[1], and Pei-De Han(韩培德)[1,‡]

[1] *College of Materials Science and Engineering, Taiyuan University of Technology, Taiyuan* 030024, *China*
[2] *Instrumental Analysis Center, Taiyuan University of Technology, Taiyuan* 030024, *China*
[3] *Taiyuan Iron and Steel (Group) Company Ltd, Taiyuan* 030024, *China*
[4] *School of Metallurgy, Northeastern University, Shenyang* 110167, *China*

(Received 28 February 2022; revised manuscript received 26 May 2022; accepted manuscript online 29 May 2022)

Precipitation in super-austenitic stainless steels will significantly affect their corrosion resistance and hot workability. The effects of Cr and Mo on precipitation behaviors were mainly achieved by affecting the driving force for precipitation, especially Mo has a more substantial promotion effect on the formation of the σ phase than Cr. In the present study, B addition to the S31254 super-austenitic stainless steels shows an excellent ability to inhibit precipitation. The effect of B on the precipitation behaviors was investigated by microstructure characterization and theoretical calculations. The experimental observation shows that the small addition of B inhibits the formation of the σ phase along grain boundaries and changes from continuous to intermittent distribution. Moreover, the inhibitory effect increased obviously with the increase of B content. The influence of B addition was theoretically analyzed from the atomic level, and the calculation results demonstrate that B can inhibit the formation of σ phase precipitates by suppressing Mo migration to grain boundaries. It is found that B and Mo are inclined to segregate at $\Sigma5$ and $\Sigma9$ grain boundaries, with B showing the most severe grain boundary segregation tendency. While B distribution at the grain boundary before precipitation begins, the segregation of Mo and Cr will be restrained. Additionally, B's occupation will induce a high potential barrier, making it difficult for Mo to diffuse towards grain boundaries.

Keywords: super-austenitic stainless steel, precipitate, segregation, boron

PACS: 64.75.Op, 68.35.bd, 73.20.–r, 63.20.dk **DOI:** 10.1088/1674-1056/ac744a

1. Introduction

Super-austenitic stainless steels (SASS) have the potential for use in extremely harsh service environments, such as flue gas desulphurization, seawater desalination, and petrochemical industry, due to high alloying elements content.[1–3] However, high content alloying elements, especially Cr and Mo, will segregation towards grain boundaries (GBs) and significantly induce the precipitation along GBs during hot working process. The precipitates of the second phase negatively affect its pitting resistance and deteriorate its mechanical properties.[4,5] Therefore, segregation of elements at GBs is one of the most critical problems in SASS because of its pronounced influence on corrosion resistance and mechanical properties. As an essential alloying element in SASS, Mo can significantly improve pitting and crevice corrosion resistance in reductive and chloride-based media. S31254 (6-wt% Mo) is one of the most important SASS because its excellent corrosion resistance compares favorably with nickel-base alloys. Due to the low solubility of Mo in austenite, it is more likely to induce Mo segregation at GBs and promote the formation of intermetallic phases like σ, χ, and Laves phase precipitation during hot working process.[6–8] Most of the second phases are hard and brittle. Their formation often causes a depleted zone of Mo and Cr in the surrounding matrix, which seriously damages the local corrosion resistance of SASS.[9,10]

As is known to all, there are many reports on improving segregation to avoid precipitation during the manufacturing process, such as alloying.[11–15] However, few studies have reported the improvement such as by adding B, in particular, it is not clear how B affects precipitation at GBs. As an efficient method, addition of a small amount of B (typically 3 wt%–30 wt% ppm) to stainless steels and low-alloy steels can significantly inhibit the nucleation of the second phases.[16,17] The reason for such an improvement has been frequently attributed to segregation of B at (prior) austenite grain boundaries (PAGBs), which may reduce the GB energy. Depending on the thermal cycle (soaking temperature, cooling rate, and final cooling temperature), B segregation can be controlled either by equilibrium (equilibrium segregation, ES) or non-equilibrium mechanisms (non equilibrium segregation, NES).[18,19] It has been claimed that the segregation

†Corresponding author. E-mail: majinyao@tyut.edu.cn
‡Corresponding author. E-mail: hanpeide@tyut.edu.cn

© 2022 Chinese Physical Society and IOP Publishing Ltd

of B may fill vacancies at GBs, thus decreasing the GB diffusivity. Moreover, it can combine with elements such as Fe or Mo to form borides; however, their precise composition and crystallography remain in doubt. The direct observation of B segregation at prior austenite GBs has been performed using the alpha-ray track etching (ATE) method and secondary ion mass spectroscopy (SIMS).[20–22] Both analysis methods are susceptible to B segregation, but quantitative the amount was complex and difficult. In addition, because B's atomic radius and mass are small, it is very difficult to observe the occupation of B atoms in experiments, and it is more difficult to explain the interaction law between B and other segregated elements. Due to the limitation of experimental technology, the atomistic behaviors of B at austenite GBs are still unclear.

For a recent review, first-principles based on density functional theory (DFT) have been the most helpful tool for investigating GB segregation and cohesive strength. During the last decade, the most theoretically studied element is S. By first-principles calculation, S is predicted to segregate to Ni GBs and cause the embrittlement, which is in perfect agreement with the experiment data.[23,24] However, the effects of B addition on the precipitation initiation and grow-up mechanisms have not been verified. In the present work, the effect of B on GB segregation of Mo and Cr during the high-temperature aging process is investigated via a combined experimental and modeling approach using first-principles method. A small B addition could improve the precipitation behaviors of precipitates, which would minimize the Mo and Cr segregation at austenite GBs. A thoroughly systematic study on the formation of σ phase in S31254 and the role of B from the atomic level was carried out. This is very important for the researchers to further understand the element segregation mechanism in SASS and the interaction between B–Mo–Cr. Similarly, it also provides a theoretical method for inhibiting precipitation and improving thermo-plasticity by adding alloy elements in production.

2. Methodology

2.1. Experimental methods

A vacuum induction furnace smelts the steels, and the main chemical composition is given in Table 1. These samples are marked as S31254, S31254-20B, and S31254-40B according to the content of B, respectively. The ingot materials were heated to 1250 °C and then hot rolled into a 20-mm thick plate. After that, the plate was cut into 10 mm×10 mm×20 mm squares using a wire cutting machine. The squares were solution treated at 1220 °C for 120 min, and then aged at 950 °C for 60 min and 120 min. In order to study the effect of B addition on precipitation, after aging treatments, the specimens were immediately water-quenched to room temperature.

Table 1. Chemical composition of experimental samples (in unit wt%).

Sample	C	Si	Mn	P	S	Cr	Ni	Mo	Cu	N	B
S31254	0.010	0.61	0.43	0.024	0.001	20.18	18.00	6.00	0.69	0.193	0
S31254-20B	0.015	0.60	0.88	0.016	0.005	20.18	18.10	6.10	0.80	0.190	0.002
S31254-40B	0.012	0.61	0.93	0.010	0.002	20.17	18.15	6.03	0.72	0.212	0.004

For microstructures observation, the surfaces of samples were polished ground by SiC papers from #180 to #3000, firstly. Then, the polished samples are etched using a solution of 10 vol.% of $HClO_4$ and 90 vol.% of CH_3COOH with a voltage of 20 V for 15 s at room temperature to obtain smooth surfaces without residual stress. In order to obtain the micro-morphology, element concentration and grain boundary character distribution (GBCD), the microstructures of samples were characterized by a JSM-7100F thermal field emission scanning electronic microscope (SEM), coupled with an electron dispersive x-ray spectroscopy (EDS) and electron backscatter diffraction (EBSD).

2.2. Computational methods

All DFT calculations[25,26] were performed using the Vienna *ab-initio* simulation package (VASP)[25] within the projector augmented wave (PAW)[27,28] approach. The Perdew–Burke–Ernzerhof (PBE)[29] was employed to describe the exchange and correlation functional. The plane wave cutoff energy was set to 400 eV. The Brillouin zone integration was performed using the Monkhorst–Pack scheme[30] for GBs. The convergence criterion of the Hellmann–Feynman force and total energy for all calculations were set as 0.01 eV/Å and 10^{-5} eV per atom, respectively. To verify the rationality of the parameter settings, the lattice constant of fcc-Fe is calculated firstly, which is 3.43674 Å after structural optimization, similar to other calculation results.[31–33] Since the atomic radius of elements such as Mo is relatively large, the alloy elements other than B are placed in the corresponding substitutional position for the following calculation. And B atoms are located in the GBs gap and octahedral interstitial space in other regions.

It is crucial to assess the segregation ability of an alloying atom (B, Mo, Cr, Ni, Mn, and Si) by its segregation energy E_{seg}, which is defined as[34]

$$E_{\text{seg}} = E_{\text{GB}}^{\text{X}} - E_{\text{bulk}}^{\text{X}}, \tag{1}$$

where E_{GB}^{X} is the energy of GB containing an alloying atom X

in different specific site, $E^{\mathrm{X}}_{\mathrm{bulk}}$ is the energy of the doped GB by an alloying atom X in the bulk site, which is located at approximately half-way between the GB plane and upper/lower interface.

The solution energy E_{sol} of atoms such as Mo in undoped GB is defined as[35,36]

$$E_{\mathrm{sol}} = E_{\mathrm{GB}}^{(N-1)\mathrm{Fe+Mo}} - E_{\mathrm{GB}}^{\mathrm{Fe}} + E^{\mathrm{Fe}} - E^{\mathrm{Mo}}, \tag{2}$$

where $E_{\mathrm{GB}}^{(N-1)\mathrm{Fe+Mo}}$ and $E_{\mathrm{GB}}^{\mathrm{Fe}}$ are the total energies of the GB supercell with and without the single substitutional Mo atom, respectively. E^{Fe} and E^{Mo} are the energies of an Fe atom and an Mo atom in their ground state, respectively. Here a smaller E_{sol} indicates that the Mo atom prefers to segregate in the related site.

In order to shed light on the stability of Mo at the GB, the solution energy can be decomposed into two contributions.[36] One is the deformation energy induced by Mo dissolution and called the structure-optimization contribution ($E^{\mathrm{str}}_{\mathrm{sol}}$), which is defined as the released energy after Mo was removed,

$$E^{\mathrm{str}}_{\mathrm{sol}} = E_{\mathrm{GB}}^{[(N-1)\mathrm{Fe+Mo}]-\mathrm{Mo}} - E_{\mathrm{GB}}^{(N-1)\mathrm{Fe}}, \tag{3}$$

where $E_{\mathrm{GB}}^{[(N-1)\mathrm{Fe+Mo}]-\mathrm{Mo}}$ and $E_{\mathrm{GB}}^{(N-1)\mathrm{Fe}}$ represent the energies of the Mo-induced distorted supercell after a substitutional Mo atom was removed and the relaxed pure GB supercell after the corresponding Fe atom was removed, respectively. The other one is the variation of electronic bonds between Mo and neighboring Fe atoms (without atomic structure optimization), and called the electronic bond contribution ($E^{\mathrm{ele}}_{\mathrm{sol}}$), which can be calculated by subtracting $E^{\mathrm{str}}_{\mathrm{sol}}$ from the solution energy of Mo,

$$E^{\mathrm{ele}}_{\mathrm{sol}} = E_{\mathrm{sol}} - E^{\mathrm{str}}_{\mathrm{sol}}. \tag{4}$$

The strengthening energy E_{str} based on Rice–Wang model can be used to examine the strengthening/embrittlement potency of impurity atoms at GBs.[37,38] Taking the undoped GB as an example, for the substitutional case, the strengthening energy E_{str} can be obtained by

$$E_{\mathrm{str}} = \left(E_{\mathrm{GB}}^{(N-1)\mathrm{Fe+X}} - E_{\mathrm{GB}}^{\mathrm{Fe}}\right) - \left(E_{\mathrm{FS}}^{(N-1)\mathrm{Fe+X}} - E_{\mathrm{FS}}^{\mathrm{Fe}}\right), \tag{5}$$

while for the interstitial case, it is defined as

$$E_{\mathrm{str}} = \left(E_{\mathrm{GB}}^{\mathrm{Fe+X}} - E_{\mathrm{GB}}^{\mathrm{Fe}}\right) - \left(E_{\mathrm{FS}}^{\mathrm{Fe+X}} - E_{\mathrm{FS}}^{\mathrm{Fe}}\right), \tag{6}$$

where $E_{\mathrm{FS}}^{\mathrm{Fe}}$ and $E_{\mathrm{FS}}^{(N-1)\mathrm{Fe+X}}/E_{\mathrm{FS}}^{\mathrm{Fe+X}}$ are the total energies of the free surface of undoped fcc-Fe and free surface with an alloying atom. The positive E_{str} indicates that the GB is weakened by the solute element, and vice versa.

3. Results and discussion

3.1. Effect of B on precipitates of S31254

To analyze the effect of B on the precipitation during the aging process in SASS, three kinds of samples after being solution treated at 122 °C for 120 min and aging at 950 °C were characterized by SEM. Figure 1 demonstrates the microstructure of S31254, S31254-20B, and S31254-40B aged for 60 min and 120 min, respectively. It can be seen that the precipitates are mainly precipitated at the austenite boundaries except the twin boundaries. Furthermore, the content of B has a significant effect on precipitates inhibition, and the number of precipitates decreases obviously with the increase of B content. On the other hand, the number of precipitates increases with the extension of aging time. Specifically, after aging for 60 min, continuous precipitates have formed along GBs in S31254 (as shown in Fig. 1(a)). For S31254-20B, the number of precipitates decreases obviously, and the fine precipitates are distributed discontinuously along GBs, as shown in Fig. 1(b). With the increase of B content, the discontinuity of precipitates increases and there are very few precipitates at the GBs of S31254-40B (as shown in Fig. 1(c)). The results indicate that the B addition inhibits the formation of precipitation along GBs. When the aging time reaches 120 min, the number of precipitates increases obviously (as shown in Fig. 1(d)). The precipitates in S31254-20B and S31254-40B are obviously less than in S31254 with the increase of B content (as shown in Figs. 1(e) and 1(f)). From the partial enlarged detail of SEM, the discontinuity of precipitates increases obviously with the B content in Fig. 1.

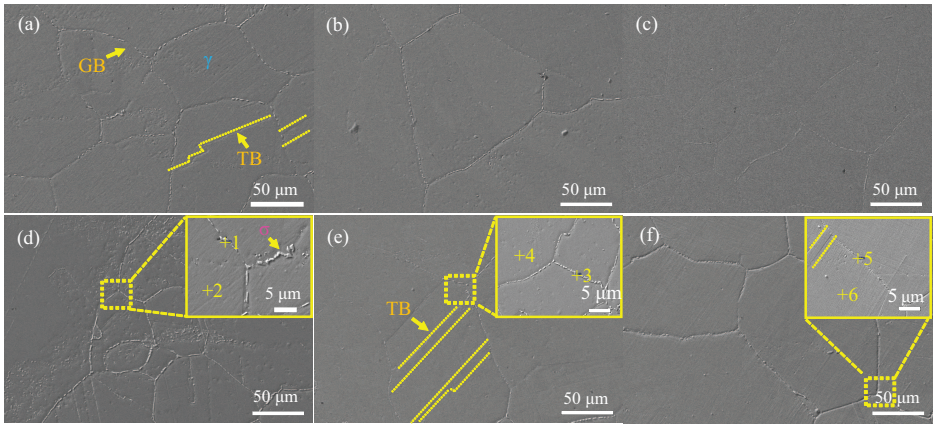


Fig. 1. The SEM of S31254, S31254-20B, and S31254-40B after aging at 950 °C for 60 min and 120 min: (a) 0B-60 min, (b) 20B-60 min, (c) 40B-60 min, (d) 0B-120 min, (e) 20B-120 min, and (f) 40B-120 min, respectively.

Table 2. The element contents (wt%) of matrix and precipitates in S31254, S31254-20B, and S31254-40B after aging at 950 °C for 120 min.

Sample	Point	Fe	Cr	Mo	Ni	Si	Mn
S31254	1	39.39	24.51	25.71	8.35	1.05	0.98
	2	50.44	22.52	5.82	20.24	0.58	0.41
S31254-20B	3	45.11	22.03	18.91	11.85	1.19	0.92
	4	51.29	22.63	6.83	17.93	0.57	0.75
S31254-40B	5	47.04	20.77	14.42	14.46	0.95	2.36
	6	50.73	23.45	6.55	17.88	0.56	0.83

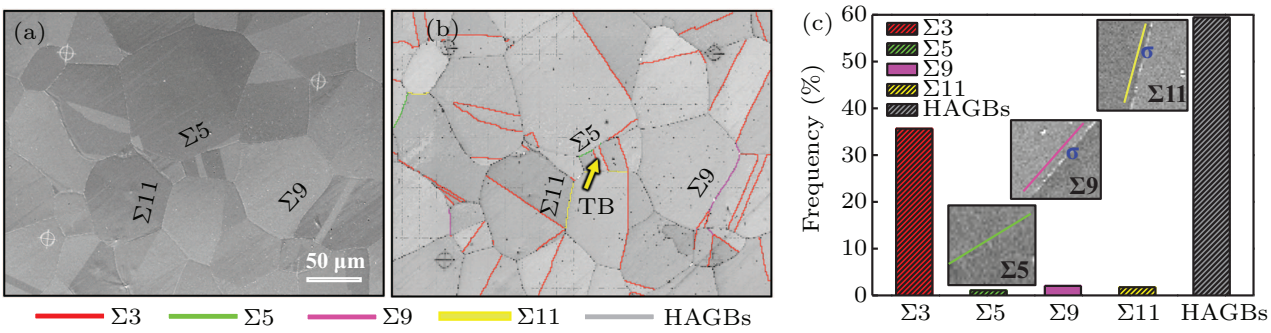


Fig. 2. (a) SEM, (b) GBCD, and (c) coincidence site lattice GBs frequency of S31254-40B, respectively.

To further characterize the composition of matrix and precipitates, based on the EDS analysis results, Table 2 provides the element contents of several points selected in the matrix and precipitates of S31254, S31254-20B, and S31254-40B after aging at 950 °C for 120 min. The results show that the main components of precipitates are Fe, Mo, and Cr in all kinds of samples, and the contents of Mo and Cr in precipitates decrease remarkably with the increase of B content. However, they still account for a large proportion. Specifically, the Mo content decreased from 25.71 wt% in S31254 to 14.42 wt% in S31254-40B, and the Cr content decreased from 24.51 wt% in S31254 to 20.77 wt% in S31254-40B. The results indicate that B can reduce the contents of Mo and Cr in precipitates.

Figure 2 presents the microstructures of S31254-40B after aging at 950 °C for 120 min. The austenitic matrix is mainly composed of random GBs. Moreover, several annealed twins are observed, and most annealed twins penetrate the entire individual grain or terminate within a single grain (Fig. 2(b)). As shown in Figs. 2(b) and 2(c), the GB types in S31254-40B are mainly Σ3, Σ5, Σ9, and Σ11, in which Σ3 GBs have the highest proportion of about 35%, and the ratio of other low-energy GBs is relatively low (only about 5%), while the rest are random high angle grain boundaries (HAGBs), and its ratio is about 6%. In addition, the Σ3 GBs are mainly coherent Σ3 twin boundaries characterized by parallel straight pairs or single lines, which localize in single grains and cannot make any positive contribution to tailoring the network of arbitrary HAGBs. In combination with Fig. 2(a), there are no precipitates at the Σ3 twin boundaries, while different amounts of precipitations appear at other Σ3 GBs, and Σ9 and Σ11 GBs.

The experimental results demonstrate that B inhibits the precipitation nucleation and growth at the austenite boundaries except the twin boundaries in SASS. Therefore, it is necessary to study the effect of B on Mo segregation at GBs. Considering the difficulty of B observing through experiment, seven types of GB structures, combined with the experimental results, were constructed. The present study focuses on B's segregation behaviors and the effect of B on GB segregation of Mo, Cr and other alloy elements, based on DFT.

3.2. Segregation behaviors at GBs

The symmetric tilt GBs are modeled based on coincidence site lattice (CSL).[39,40] In Fig. 3, seven GBs including Σ3 (111), Σ3 (112), Σ5 (210), Σ5 (310), Σ9 (114), Σ9 (221), and Σ11 (113) GBs are investigated. $1\times1\times2$ (96 Fe atoms), $2\times2\times2$ (96 Fe atoms), $1\times1\times2$ (80 Fe atoms), $1\times1\times2$ (80 Fe atoms), $1\times1\times2$ (68 Fe atoms), $1\times1\times2$ (68 Fe atoms), and $1\times1\times2$ (68 Fe atoms) supercells were used for these GBs to simulate the alloying effect, respectively. The convergence test shows that the supercell size of each GB is sufficiently large to produce a realistic result. The larger alloying atoms (Mo, Cr, Ni, Mn, and Si) occupy the substitutional sites in lattice and at the interface. In contrast, the B atoms are located in the GBs gap and octahedral interstitial space for subsequent calculations. Due to the invisibility of many interstitial sites of B from the visual angle of Fig. 3, they are not marked in the figure.

Figure 4 shows the segregation energies (E_{seg}) of B, Mo, Cr, Ni, Mn, and Si atoms in different interstitial or substitutional sites of the seven symmetric tilt GBs. As mentioned above, the negative E_{seg} indicates that the alloying atom prefers to stay at the GB. The results show that appreciable

distinction could be revealed among the segregation tendencies of B, Mo, Cr, Ni, Mn, and Si at the seven GBs. It is worth noting that B and Mo do not segregate at the Σ3 (111) twin boundaries, and the calculated result is consistent well with the distribution of the precipitates observed in Fig. 2(a), with no precipitates at Σ3 (111) twin boundaries. For the other GBs, B, and Mo exhibit much stronger segregation tendencies, especially B, and their segregation tendencies to GBs are Σ9 (211)>Σ9 (114)>Σ5 (310)>Σ5 (210)>Σ3 (112)>Σ11 (113). Mo is apt to segregate to Σ5 (310), Σ9 (221), Σ9 (114), and Σ5 (210) GBs and their adjacent areas. Cr mainly segregate to Σ5 (310) GB, Ni and Si mainly segregate to Σ9 GBs, while Si does not segregate to Σ5 (310) GB. From the SEM of S31254, S31254-20B, and S31254-40B in Fig. 1 and the EDS results in Table 2, σ phase contains high content of Mo and Cr, especially Mo. As shown in the calculation results of Fig. 4, Mo exhibits the strongest segregation tendency among the substitutional alloying elements, and it is apt to segregate to Σ5 and Σ9 GBs, which is consistent with the results of Fig. 1. It can be clearly seen from Fig. 1 that there are numerous precipitates at the GBs except twin boundaries.

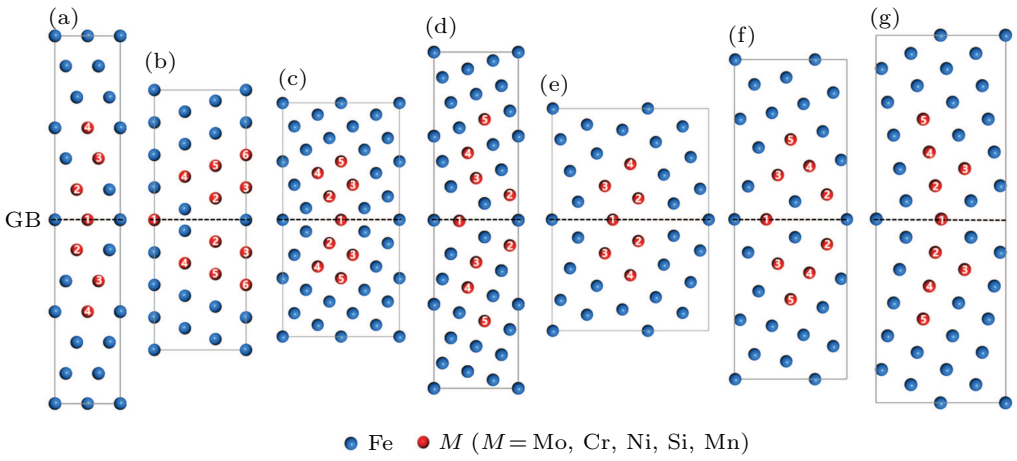


Fig. 3. Schematic structures of symmetric tilt GBs: (a) Σ3 (111), (b) Σ3 (112), (c) Σ5 (210), (d) Σ5 (310), (e) Σ9 (114), (f) Σ9 (221), and (g) Σ11 (113), respectively. The atomic sites for substitution are marked in red.

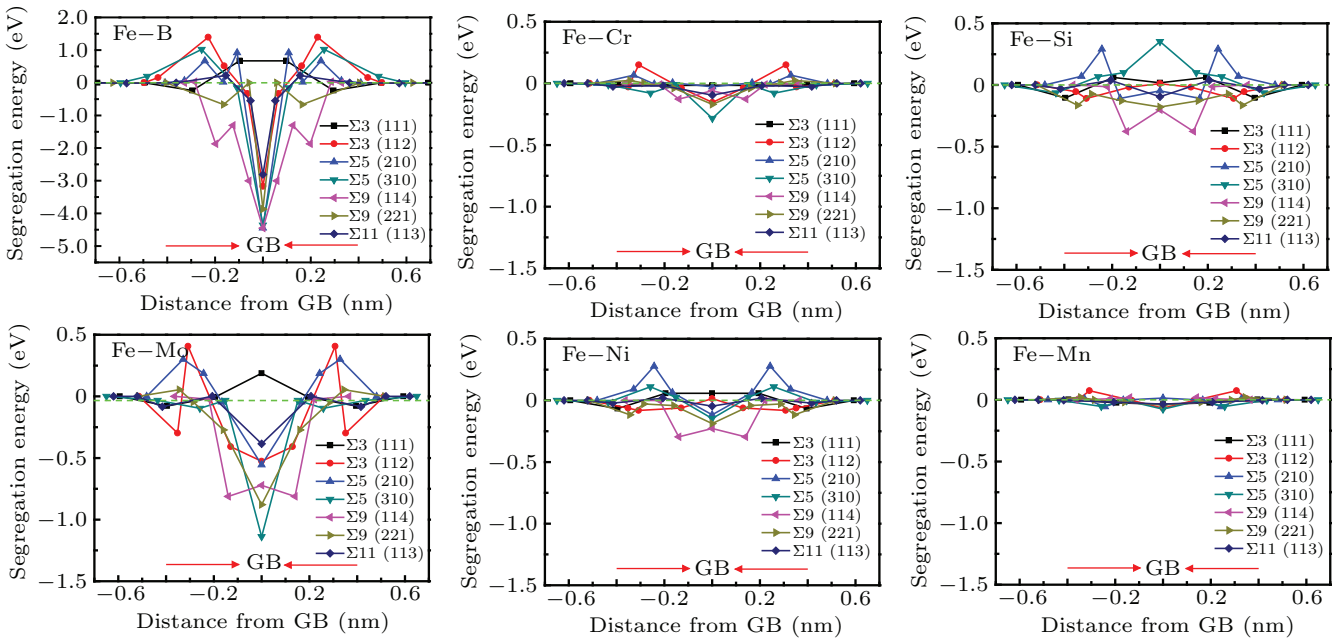


Fig. 4. Segregation energies *versus* the distance from GB plane for B, Mo, Cr, Ni, Mn, and Si at Σ3 (111), Σ3 (112), Σ5 (210), Σ5 (310), Σ9 (114), Σ9 (221), and Σ11 (113) GBs, respectively.

3.3. B effect on GB segregation tendencies of Mo

B and Mo are easy to segregate to GBs from the above calculation results. According to the current experimental in Fig. 2, Σ3, Σ5, and Σ9 are the three most common GB types in austenitic stainless steels.[41,42] The segregation of Mo leads to σ phase formation, and the content of Cr in σ phase is also higher than that in the matrix. So, figures 5(a)–5(c) depict the segregation energies of Mo and Mo–Cr at Σ3 (112), Σ5 (210), and Σ9 (114) GBs with different distances from the GB plane when B locates at these GBs. The results show B can inhibit

the segregation of Mo. The most substantial inhibitory effect appears at Σ3 (112) GB. At the same time, the segregation energies of Mo near the GB become positive values when B locates at Σ3 (112) GB, indicating a very high potential barrier appears around the GB, which can improve the difficulty of Mo diffusing to Σ3 (112) GB. Similarly, B can also inhibit the segregation of Mo to Σ5 (210) GB, resulting in a significant increase in the segregation energy of Mo at the GB and a high potential barrier around it. Although B only shows a slight inhibitory effect on Mo segregating to Σ9 (114) GB, it also induces a very high potential barrier. According to the calculation results, figures 5(a)–5(c) also describes the impact of B on the segregation energies of Mo–Cr co-segregation at Σ3 (112), Σ5 (210), and Σ9 (114) GBs when B locates at these GBs. It shows that the segregation caused by the Fe–Cr–Mo composite configuration when Cr and Mo coexist at these GBs is not as severe as when Mo exists alone. B can inhibit the co-segregation tendency of Mo–Cr at the three GBs, especially Σ9 (114) GB. Although there is still tiny segregation of Cr and Mo to Σ3 (112) GB when B locates at the GB, a very high potential barrier also appears around the GB to improve the difficulty of Cr and Mo segregation. In general, when B locates at GBs, it can retard and delay the precipitation of the σ phase at GBs, especially Σ3 (112) and Σ5 (210) GBs. In combination with Fig. 2, it can be seen that there are no precipitates at Σ3 and Σ5 GBs, while precipitates still appear at Σ9 GB.

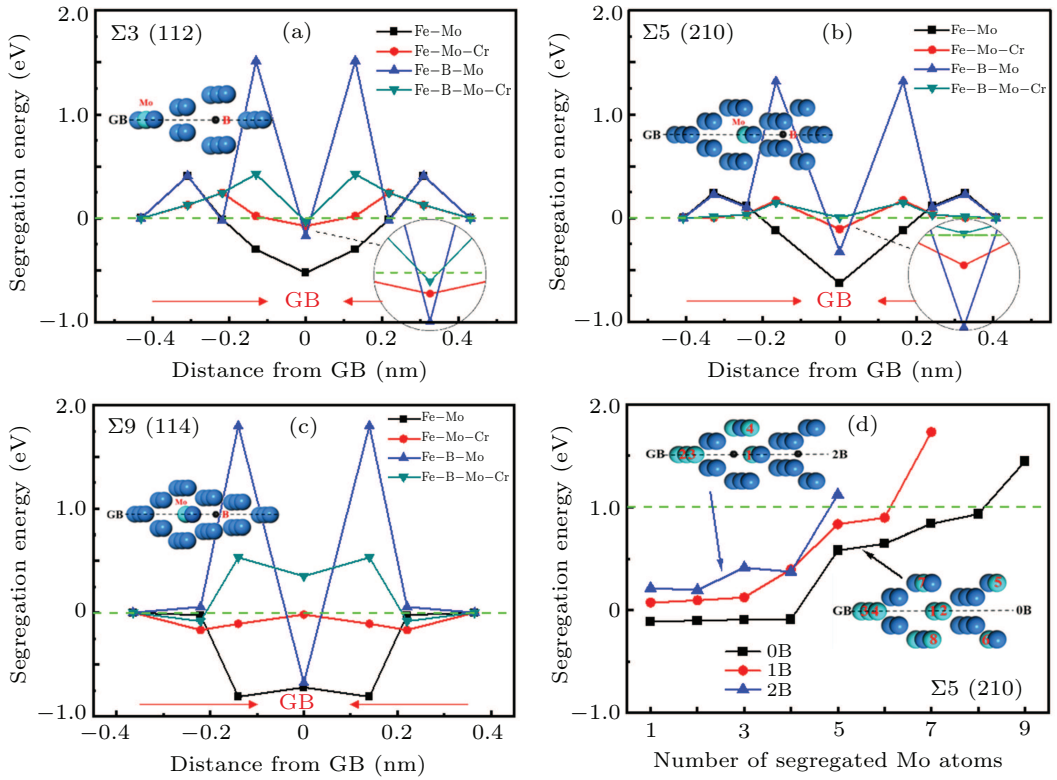


Fig. 5. (a)–(c) Segregation energies *versus* the distance from GB plane for Mo, Mo–Cr at Σ3 (112), Σ5 (210), and Σ9 (114) GBs when B locates at these GBs, respectively; (d) segregation energies of multiple Mo atoms at Σ5 (210) GB and its adjacent area *versus* the number of Mo atoms, with different B contents.

The segregation behaviors of multiple Mo atoms at GBs and in the adjacent areas of GBs were investigated by considering different B contents. To clear the most stable configuration of Mo atoms at GBs, figure 5(d) delineates the segregation energies of multiple Mo atoms at Σ5 (210) GB and in its adjacent area as a function of the number of Mo atoms, with different B contents. It is found that the segregation energy of Mo is basically unchanged when only fewer Mo atoms (< 4) segregate, which indicates multiple Mo atoms can segregate together easily. While the segregation energy shows, a noticeable step-like jump increases with the number of Mo atoms at GB increasing (> 4), which means their segregation tendency gradually weakens. The segregation energy changes from negative to positive when the number of Mo atoms reaches 9, indicating that it is difficult for many Mo atoms to segregate together. The 9th and subsequent Mo atoms prefer to occupy the substitutional site in bulk rather than the GB region. In other words, the number of segregated Mo atoms in the GB region has reached the upper limit. More importantly, the results indicate that the number of B atoms obviously affects Mo segregation. When Σ5 (210) GB contains one B atom, the segregation energy of Mo also increases with the number of segregated Mo atoms increasing. Still, the values are greater than those of the GB without B, and the upper limit of the number

of segregated Mo atoms in the GB region is only 6. When the GB contains two B atoms, the segregation energy of Mo increases obviously, and the upper limit of the number of segregated Mo atoms in the GB region is only 4. The result means that the segregation tendency of Mo is significantly weakened and the difficulty of Mo segregating increases prominently. In summary, B can inhibit Mo from segregating to GBs and their adjacent areas, and the inhibitory effect becomes more evident with higher B content.

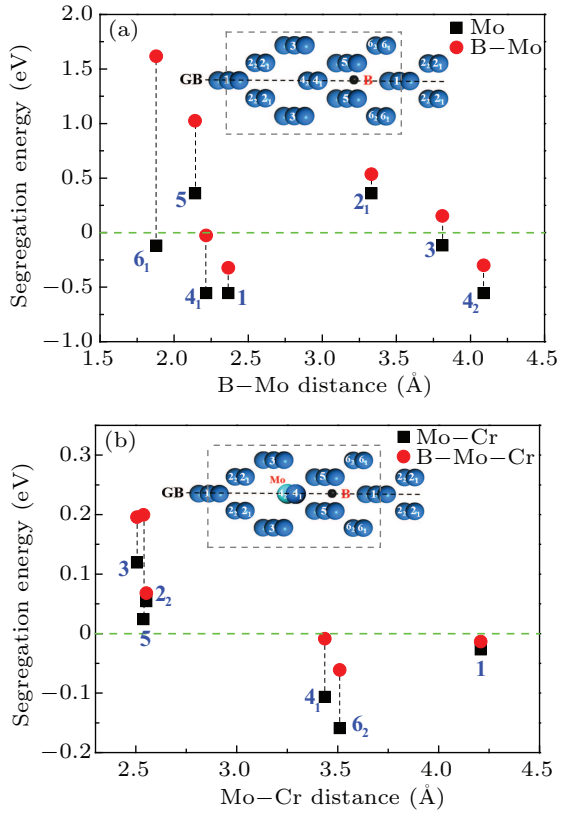


Fig. 6. (a) Segregation energies of Mo at Σ5 (210) GB and in its adjacent area as well as the effect of B; (b) effect of Mo and Mo–B on the Cr segregation when they occupy their optimum segregation sites.

To further analyze the effect of B on Mo and Cr segregation at GBs and in their adjacent areas, the most representative Σ5 (210) GB in the above experiments was selected for element occupation analysis. When B occupies its optimum segregation position, the symmetry of the substitutional sites at Σ5 (210) GB and its adjacent area will change, so those substitutional sites are anew represented by x_n later. For example, according to symmetry, site 1 is still unique, while site 2 is divided into two distinct positions, 2_1 and 2_2. Figure 6(a) reveals the segregation energies of Mo at Σ5 (210) GB and in its adjacent area and the effect of B. It can be found that there are two effects of B on Mo segregation: the environment of the substitutional site and the distance from B. After B addition, the segregation energies of Mo in site 1 and site 4_2 are the lowest due to the appropriate distance and suitable segregation environment. Still, Mo is difficult to diffuse to site 2_1 and 5 because of the limited environment. And Mo does not segregate to site 6 and site 4_1 near B. Figure 6(b) gives the effect of Mo and Mo–B on the Cr segregation when they occupy their optimum segregation sites. It can be found that after B addition, the segregation energies of Cr increase. In particular, the segregation energies of Cr in sites 4_1 and 6_2 near B significantly increase, and the segregation of Cr towards GB is inhibited. No matter whether B is added or not, the segregation energy of Cr has the lowest value when the Cr–Mo distance is about 3.5 Å. Therefore, besides the distance from B and the environment around the substitutional site, Cr segregation is mainly related to the relative distance with Mo. In summary, B primarily first affects the occupation of Mo at GBs, and then Mo affects the distribution of Cr.

Four different alternative sites at Σ5(210) GB and in its adjacent area were selected to further analyze the effect of Mo segregation on the GB. Site 4_1 is on the plane of the GB, site 5 and 6_2 are closest to the interface, and site-matrix is the substrate position. Table 3 lists the coordination numbers, solution energies (E_{sol}), structural optimization contributions, and electronic contributions of solution energies when Mo is located at the four alternative sites. The coordination numbers of site 4_1 and site-matrix are both 12, and those of site 5 and 6_2 are 10 and 11, respectively. The average most adjacent distances from site to neighboring Fe atom of site 4_1, 5, and 6_2 are 2.482 Å, 2.362 Å, and 2.428 Å, respectively. The average most adjacent distances of site 4_1 is the largest and its corresponding polyhedron volume is also the largest among the three sites. When B locates in the GB region, the solution energy of Mo in site 4_1 is still the lowest, so site 4_1 is the most stable segregation site for Mo segregating to Σ5 (210) GB. Except for site 5, B can improve the solution energy of Mo in each site, especially site 6_2. The structural optimization contributions of all solution energies are all negative, indicating that the structural distortion caused by Mo segregation positively affects Mo segregation. While the electronic contributions are positive values, the electron interaction between segregated Mo and its neighboring Fe atom is detrimental to Mo segregation. After B addition, the structural optimization contributions of all solution energies decrease. The reason is that B segregation causes the lattices at the GB to expand, increasing the usable volume of GB. Therefore, B segregation is advantageous to Mo segregation from the structural point of view. After B addition, the electronic contributions of all solution energies increase significantly, indicating that the electron interaction between the segregated Mo and its neighboring Fe atom is an unfavorable factor for the strength of the GB containing B.

Based on the Rice–Wang thermodynamic model, the strengthening energies of Σ5 (210) GBs are calculated to analyze the effects of Mo, B, and Mo–B segregation on the interface bonding. The strengthening energies of GB containing B,

GB containing Mo, and GB containing Mo–B are −0.691 eV, 0.401 eV, and 1.096 eV, respectively. Therefore, B improves the interfacial binding ability, while Mo segregation and Mo–B co-segregation both reduce it.

Charge density distributions analysis was performed to analyze the interaction among atoms visually. Figure 7 displays the charge density distributions of pure and segregated Σ5 (210) GBs with 0% and 12% tensile deformation in Fe, Fe–B, Fe–Mo, and Fe–Mo–B systems. From Fig. 7(a), compared with the pure fcc-Fe GB, although B segregation enlarges the distance between the upper and lower Fe atoms at Σ5 (210) GB, the atomic charge at the GB is supplemented, and the original common charge density area disappears. Combined with the strengthening energies, the chemical effect caused by the increase of the local charge density attributed to the electronic structure after B segregating to Σ5 (210) GB exceeds the adverse impact caused by the structural change, which improves the interfacial bonding ability. Mo segregation enlarges the atomic distance at the GB and expands the structure, and the original low charge density area still exists, which reduces the interfacial bonding ability. Although Mo–B co-segregation partially compensated the atomic charge at the GB, the atomic distance increases significantly. The increase of local charge density is not enough to offset the adverse effect of structural change. Figure 7(b) illustrates the charge density distributions of Σ5 (210) GB system after uniform stretching by 12%. It can be found that after 12% stretching, the original low charge density area at the GB without B is significantly enlarged, indicating that GBs are the weakest parts of the materials, and the materials will fracture from the GB interfaces when the deformation increases. After B locating at the GB, B segregates to the interstitial sites of the GB and expands the charge distribution area at the GB. In particular, the GB structure after tensile deformation remains intact, and B improves its surrounding charge density and significantly enhances GB's interfacial binding ability. After stretching, the structure of the GB containing Mo expands more obviously, and the low charge density area still exists. Mo–B co-segregation supplements the charge at GB, but it produces more significant expansion deformation of GB.

Table 3. Coordination numbers, solution energies (in unit eV), and the structural optimization contributions (in unit eV), and electronic contributions (in unit eV) of the solution energies of Mo in the alternative sites at Σ5 (210) GB and in its adjacent area.

	Coordination number	0B			1B		
		E_{sol}	E_{sol}^{str}	E_{sol}^{ele}	E_{sol}	E_{sol}^{str}	E_{sol}^{ele}
Site-4_1	12	–0.197	–11.0	10.8	0.184	–13.2	13.4
Site-5	10	0.867	–8.01	8.88	0.802	–8.74	9.54
Site-6_2	11	0.313	–11.8	12.1	1.826	–13.4	15.2
Site-matrix	12	0.359	–12.3	12.7	0.467	–14.6	15.1

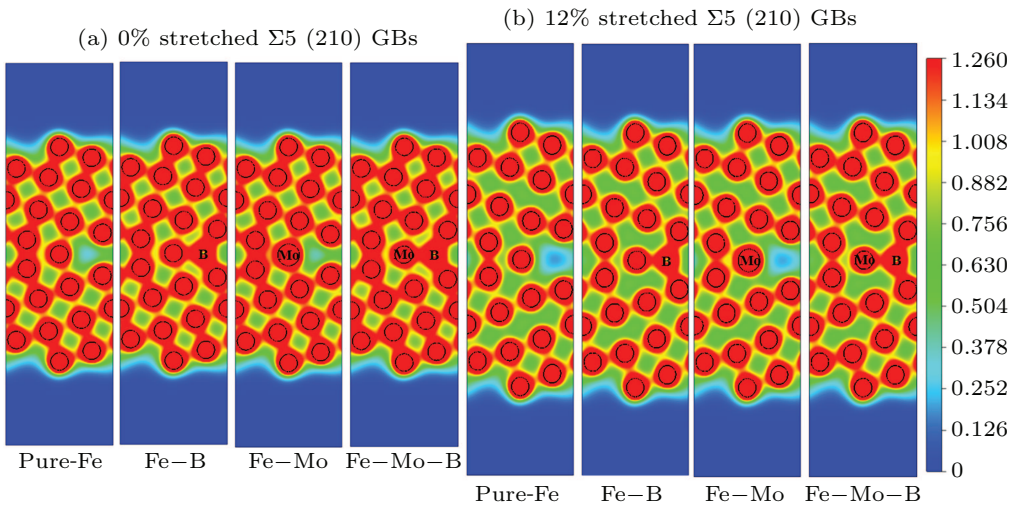


Fig. 7. Charge density distributions of pure and segregated Σ5 (210) GB with 0% and 12% tensile deformations.

Due to the extremely low solubility (usually several wt. ppm) of B in austenite,[43] so it is more easily to segregate to GBs. When B is distributed at GBs, it will regulate the segregation of alloying elements to GBs. In combination with Fig. 1, with the increase of B addition to S31254 SASS, less and less σ phase precipitates to GBs, meanwhile, the discontinuity of precipitated σ phase increases. The results indicate that the B addition inhibits the formation of σ phase. Besides, according to the reported results,[44] when no B was added to austenitic stainless steel, Cr-poor zone would form in the matrix of stainless steel. However, no depleted zone of Cr appears in our austenitic stainless steel samples containing B, which

indicates that the Cr-depletion no longer exists in matrix and the adjacent area of GBs.

Figure 8 exhibits the schematic element segregation process before nucleation for σ phase in SASS without and with B at GB. Cr, Mo, and Ni atoms in SASS are randomly distributed in the matrix, and B atoms are distributed at GB under solution conditions (Figs. 8(a) and 8(c)). When there is no B at GB, Mo and Cr atoms migrate and concentrate to the GB region during aging treatment. And the co-segregation of Mo–Cr atoms forms large-scale element concentration areas, as shown in the GB region of Fig. 8(b). Cr-depletion and Mo-depletion induced by Mo–Cr co-segregation, as shown in the black dashed rectangular region of Fig. 8(b). The B segregated to GB inhibits the segregation of Mo and Cr to GB region near B, so Mo will segregate to those regions far from B, and Cr will segregate around Mo, which is shown in the GB region of Fig. 8(d). It is not easy to form a continuous σ phase at GB because of the distribution of Cr and Mo, and only the discontinuous σ phase can be formed far from B. In addition, the Cr-depletion no longer exists in the adjacent area of the GB, as shown in the black dashed rectangular region of Fig. 8(d).

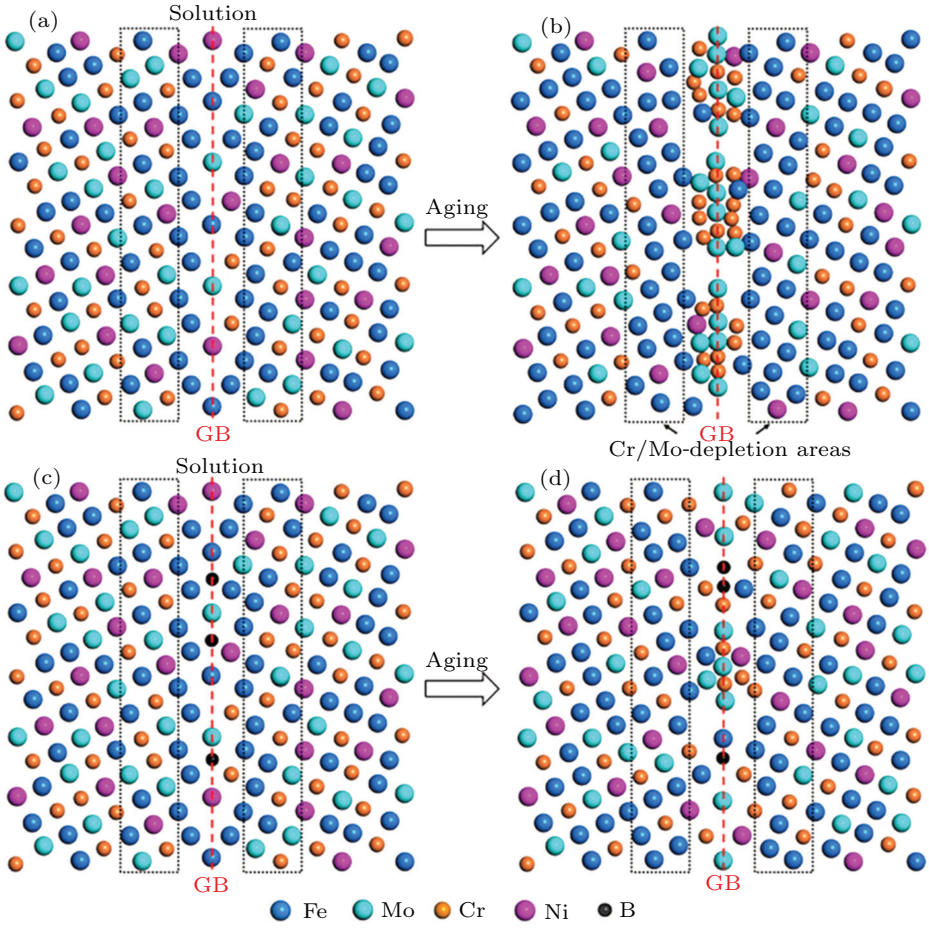


Fig. 8. Schematic illustration of element segregation process before nucleation for σ phase in SASS [(a)–(b)] without B and [(c)–(d)] with B at GB, respectively. (a) and (c) Random segregation of Fe, Mo, Cr, and Ni atoms at GB; (b) and (d) co-segregation of Mo and Cr atoms at GB, respectively.

4. Conclusions

Narrative analysis for the precipitation law of the σ phase in SASS without and with B was combined with the experiments and simulation calculations. As the main elements of the σ phase, the segregation tendency of Mo and Cr at seven symmetric tilt GBs and the role of B were discussed from the atomic level. The results are as follows:

(i) In the S31254 SASS aged at 950 °C, the σ phase preferentially precipitates along GBs, and the number of precipitates increases with the extension of aging time. B can inhibit the precipitation of σ phase at GBs and reduce the number of precipitates.

(ii) Combining with experiments, seven symmetric tilt GBs of Σ3 (111), Σ3 (112), Σ5 (210), Σ5 (310), Σ9 (114), Σ9 (221), and Σ11 (113) in fcc-Fe were constructed, and the occupation tendencies of B, Cr, Mo, and other atoms in these GBs were analyzed. The results show that no segregation of B and Mo is distributed at Σ3 (111) twin boundaries at all, which is in complete agreement with the experimental results of the distribution of precipitates. B and Mo are most likely to segregate to Σ5 and Σ9 GBs, especially for B, while the tendency of Cr segregating to GBs is very weak.

(iii) B preferentially occupy the GBs, inhibiting the segregation of Mo at GBs, and forming a high barrier around these GBs, which makes it difficult for Mo to migrate and diffuse to these GBs. The segregation of B at GBs is beneficial to improving the interfacial bonding ability, while Mo segregating to GBs would reduce it.

(iv) It is clarified that Cr and Mo are most likely to co-segregate at Σ3, Σ5, and Σ9 GBs from the atomic level, which is the main reason for the formation of σ phase. When B segregates to GBs, Cr and Mo's segregation tendencies to Σ3, Σ5, and Σ9 GBs would be suppressed. Therefore, the σ phase would be difficult to form in the adjacent area of B.

Acknowledgement

Project supported by the National Natural Science Foundation of China (Grant Nos. U1860204 and 51871159).

References

[1] Sathiya P, Mishra M K and Shanmugarajan B 2012 *Mater. Design* **33** 203
[2] Zambon A, Ferro P and Bonollo F 2006 *Mater. Sci. Eng. A* **424** 117
[3] Bonollo F, Tiziani A, Tovo R, *et al.* 2004 *Weld. Int.* **18** 24
[4] Mishin Y, Asta M and Li J 2010 *Acta Mater.* **58** 1117
[5] Gibson M A and Schuh C A 2015 *Acta Mater.* **95** 145
[6] Lee C, Roh S, Lee C, *et al.* 2018 *Mater. Chem. Phys.* **207** 91
[7] Hao Y, Cao G, Li C, *et al.* 2019 *Mater. Charact.* **147** 21
[8] Zhang S, Jiang Z, Li H, *et al.* 2018 *Mater. Charact.* **137** 244
[9] Wang J, Cui Y, Bai J, *et al.* 2019 *Mater. Lett.* **252** 60
[10] Zhang S, Li H, Jiang Z, *et al.* 2019 *Corros. Sci.* **163** 108295
[11] Uggowitzer P J, Magdowski R and Speidel M O 1996 *ISIJ Int.* **36** 901
[12] Simmons J W 1996 *Mater. Sci. Eng. A* **207** 159
[13] Speidel H J C and Speidel M O 2004 *Mater. Manuf. Process.* **19** 95
[14] Wang Q, Wang L, Zhang W, *et al.* 2020 *Metall. Mater. Trans. B* **51** 1773
[15] Wang Q, Wang L, Sun Y, *et al.* 2020 *J. Alloys Compd.* **815** 152418
[16] Yu J, Zhang S, Li H, *et al.* 2022 *J. Mater. Sci. Technol.* **112** 184
[17] Kurban M, Erb U and Aust K T 2006 *Scripta Mater.* **54** 1053
[18] Faulkner R G 1987 *Acta Metall.* **35** 2905
[19] He X L, Chu Y Y and Jonas J J 1989 *Acta Metall.* **37** 147
[20] Karlsson L and Norden H 1988 *Acta Metall.* **36** 13
[21] Asahi H 2002 *ISIJ Inter.* **42** 1150
[22] Takahashi J, Ishikawa K, Kawakami K, *et al.* 2017 *Acta Mater.* **133** 41
[23] Lejček P, Šob M and Paidar V 2017 *Prog. Mater. Sci.* **87** 83
[24] Razumovskiy V I, Lozovoi A Y and Razumovskii I M 2015 *Acta Mater.* **82** 369
[25] Kohn W and Sham L J 1965 *Phys. Rev. B* **140** A1133
[26] Kresse G and Furthmüller J 1996 *Phys. Rev. B* **54** 11169
[27] Blöchl P E 1994 *Phys. Rev. B* **50** 17953
[28] Kresse G and Joubert D 1999 *Phys. Rev. B* **59** 1758
[29] Perdew J P, Burke K and Ernzerhof M 1996 *Phys. Rev. Lett.* **77** 3865
[30] Pack J D and Monkhorst H J 1977 *Phys. Rev. B* **16** 1748
[31] Li Y, Han C, Zhang C, *et al.* 2016 *Comp. Mater. Sci.* **115** 170
[32] Häglund J, Guillermet A F, Grimvall G, *et al.* 1993 *Phys. Rev. B* **48** 11685
[33] Jiang D E and Carter E A 2003 *Phys. Rev. B* **67** 214103
[34] Wu X, You Y W, Kong X S, *et al.* 2016 *Acta Mater.* **120** 315
[35] Yang Y, Ding J, Zhang P, *et al.* 2019 *Nucl. Instrum. Method B* **456** 7
[36] Zhang B, Li Y H, Zhou H B, *et al.* 2020 *J. Nucl. Mater.* **528** 151867
[37] Zhang S, Kontsevoi O Y, Freeman A J, *et al.* 2011 *Acta Mater.* **59** 6155
[38] Rice J R and Wang J S 1989 *Mater. Sci. Eng. A-Struct* **107** 23
[39] Warrington D H 1975 *J. Phys. Colloq.* **36** C4-87
[40] Sutton A P and Balluffi R W 1995 *Interfaces in crystalline materials* (New York: Oxford University Press) p. 414
[41] Guan X J, Shi F, Jia Z P, *et al.* 2020 *Mater. Charact.* **170** 110689
[42] Zhou Q, Wang R, Zheng Z, *et al.* 2018 *Appl. Surf. Sci.* **462** 804
[43] Nai Q L, Zheng W J, Song Z G, *et al.* 2013 *J. Iron Steel Res.* **25** 53
[44] Wang J, Cui Y, Bai J, *et al.* 2019 *J. Electrochem. Soc.* **166** C600